



HAL
open science

Gas-liquid atomisation: gas phase characteristics by PIV measurements and spatial evolution of the spray

Michaël N. Descamps, Jean-Philippe Matas, Alain H. Cartellier

► To cite this version:

Michaël N. Descamps, Jean-Philippe Matas, Alain H. Cartellier. Gas-liquid atomisation: gas phase characteristics by PIV measurements and spatial evolution of the spray. 2nd colloque INCA, Initiative en Combustion Avancée, Oct 2008, Rouen, France. pp.1. hal-00704346

HAL Id: hal-00704346

<https://hal.science/hal-00704346>

Submitted on 5 Jun 2012

HAL is a multi-disciplinary open access archive for the deposit and dissemination of scientific research documents, whether they are published or not. The documents may come from teaching and research institutions in France or abroad, or from public or private research centers.

L'archive ouverte pluridisciplinaire **HAL**, est destinée au dépôt et à la diffusion de documents scientifiques de niveau recherche, publiés ou non, émanant des établissements d'enseignement et de recherche français ou étrangers, des laboratoires publics ou privés.

Gas-liquid atomisation: gas phase characteristics by PIV measurements and spatial evolution of the spray

M.N. Descamps, J.-P. Matas, A. Cartellier

Laboratoire des Ecoulements Géophysiques et Industriels, BP 53, 38041 Grenoble Cedex 9, France

We have investigated the atomisation of a thick liquid film by high speed co-flowing gas jet. The study is focused on the mechanisms controlling the drop spatial distribution downstream injection. These results are needed for properly initializing two-fluid euler-euler [1] or lagrangian [2] simulations.

Measurements of the drop characteristics (concentration, velocity, size), available downstream injection, indicate that the spatial dispersion of the drops is related to their size, the smallest drops being more widely spread than the larger ones. However, the standard dispersion model based on turbulent dispersion is unable to describe such a behaviour up to a downstream distance about $6 H_g$. According to the experimental results presented, the drawback may originate from the initial ejection conditions. Another origin could be a change in the gas structure (jet expansion, turbulent intensity) at short distances. The relative contributions of these mechanisms needs to be quantified.

INTRODUCTION

Gas assisted atomisation is commonly employed in various industrial processes and notably in combustion engines. The design of these injection devices is often crucial since it has strong consequences on the drop size and flux as well as on the spatial organisation of the spray. In that scope, various simulation approaches are currently under development. Some address the question of drop formation (primary atomisation) by way of direct simulations. Others are aimed at the spray description in an average sense, using either eulerian [1] or lagrangian [2] modelling frameworks. Yet, the mechanisms controlling the spray characteristics are not completely understood.

Within the atomisation zone, some progress has been made on the role of interfacial instabilities on the drop formation. However, as drops are formed and entrained by the gas, they alter the gas phase behaviour which, in its turn, can influence the atomisation process itself [3]. Also, almost no detailed information is available on the structure of a gas-liquid mixing layer which can alter the droplet ejection conditions or may possibly force drop-drop collisions.

Concerning the spatial evolution of the spray, a first issue concerns the relative role of coalescence and break-up due to drop-drop collisions and drop-turbulence interactions: that issue has been partly addressed [4]. Another key question, that has received much less attention, concerns the mechanisms controlling the lateral dispersion of droplets. In particular, it is not clear how far the initial conditions prevailing during the drop formation affect the spray structure. That issue is especially important for the correct initialisation of average two-fluid simulations.

Dedicated laboratory experiments were carried out using non-reacting, substitution fluids under ambient conditions. A data base of the dispersed phase characteristics was performed by [5]. In the present study, efforts were made toward obtaining informations about the gas phase and describing the lateral dispersion of drops.

The experimental setup and measurement techniques are briefly discussed in section I. In section II we present some velocity measurements performed in the gas phase, both for gas flow and gas-liquid flow. In section III some dispersed phase characteristics, such as the drop flux or the drop trajectories, are shown, and emphasis is then put on the dispersion mechanism in section IV.

I EXPERIMENTAL SETUP

The experimental setup consists of a two-phase planar mixing layer. We used water and air in ambient conditions (20°C and atmospheric pressure). Fluid streams are delivered through convergent rectangular cross-section nozzles (figure 1 left). At the exit of both nozzles, the transverse extension is 10 cm and the height is 1 cm (the height in the gas and liquid phase are noted respectively H_g and H_l). With this aspect ratio we neglect the influence of side walls, and ensure that the flow is bidimensional. Injection of

both fluids is made through honeycombs and with a smooth convergence (contraction ratio is 10), to ensure relatively clean flows where the intensity of perturbation and turbulence are reduced. Air and water mean velocities measurements are made respectively with a mass-flowmeter and a rotameter (Krohne).

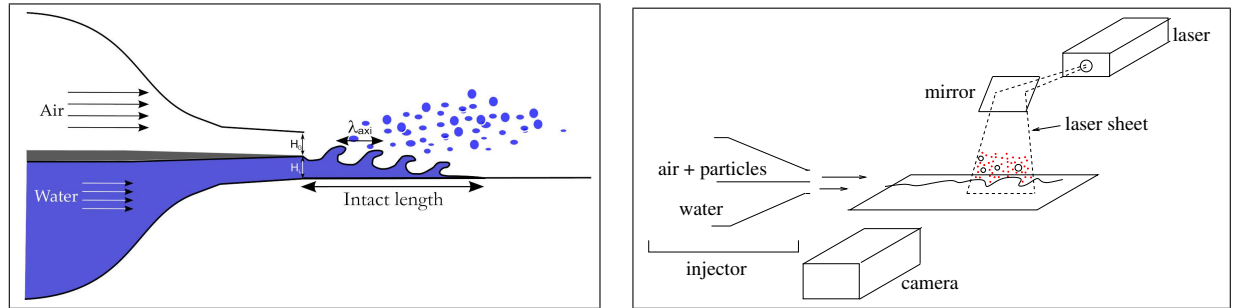


Figure 1 : Sketch of the fluids injection (left) and laser configuration (right)

In the following, the measurement techniques will be briefly discussed.

The characteristics of the dispersed phase were obtained using an optical probe. By introducing some hypothesis on the flow structure [6], it is possible to derive from the probe signal the joint probability density function (pdf) size-velocity, the number density flux of the drops φ , the local liquid phase fraction α , and the interfacial area density Γ . These quantities are also available per size classes. The detail of this system as well as some qualifications of its performance are available in [7].

One of the goals of this study is to gather data on the gaz velocity field using Particle Image Velocimetry (PIV). Therefore, tracers produced from a mixture of water and glycerin are injected in the gas flow, inside the gas convergent nozzle. In order to have consistent velocity fields, we take care that the tracers are seeded as homogeneously as possible in the measurement zone. Moreover, the tracers, which follow the gas flow, have to be discriminated from the water drops stripped off from the liquid flow. It will be seen at the end of this section that the discrimination can be made based on the velocity field.

The laser used was a Twins Ultra Yag from Quantel. The laser sheet was oriented in the longitudinal direction of the flow, as sketched in figure 1 (right).

The aquisition and processing of the PIV image was performed using the software Davies 7.2 from La Vision. The output file consists of the instantaneous gas velocity field in the laser sheet. The field resolution is in the range 0.2 mm to 0.4 mm depending on the optical enlargement. In order to have a reliable mean flow field, an average over 1500 velocity fields was performed for each flow conditions. Second order moments were also calculated, but their interpretation should be done with care. Indeed, the velocity fluctuations in the successive PIV fields can arise from the flow field itself as well as from mistakes in the PIV algorithm calculation. This is particularly true for severe conditions of flow rates. Furthermore, the software allows to process the data using Particle Tracking Velocimetry (PTV), which computes velocity of individual drops detected over a pair of image. This procedure is useful for determining the instantaneous drop velocity.

Finally, we used high-speed video recording, to obtain information on drop trajectories and the properties of the interfacial waves. A Phantom V12 camera was used, at a sampling frequency of 1000 Hz for a resolution of 1280×800 pixels.

Measurement conditions

For a dense dispersion, the image processing appeared to be unreliable. Hence, only the conditions for which the number of drops dispersed in the gas phase remained weak were considered. The gas velocity at the injection was varied in the range 13 m/s to 30 m/s, and the water velocity was varried in the range 0.1 m/s to 0.3 m/s. The images were captured in a zone downstream injection between 0 and $10H_j$. In this zone, which is relatively close to the injector, the drops are just formed and accelerated by the gas stream, but their velocity is still very different from that of the gas. This statement holds for gas velocity smaller than 30 m/s. As a consequence, it is easy to discriminate between the PIV tracers, whose displacement is large between in a pair of images, and water drops, whose displacement is virtually zero in a pair of images.

II MEASUREMENTS IN THE CONTINUOUS PHASE

II.1 SINGLE-PHASE GAS FLOW

The PIV technique was first validated in a single-phase gas flow, case for which the data of [8] and [3] can be used as a reference. At the exit of the nozzle, we observe a turbulent gas profile, of shape similar to that measured with hot-wire anemometry. The gas vorticity thickness is defined as:

$$\delta_g = \frac{\Delta U_{max}}{\left(\frac{dU}{dy}\right)_{max}} \quad (1)$$

There is a good agreement between the value of δ_g measured by PIV and the fitted expression derived by [3] from the anemometry data, as can be seen in figure 2.

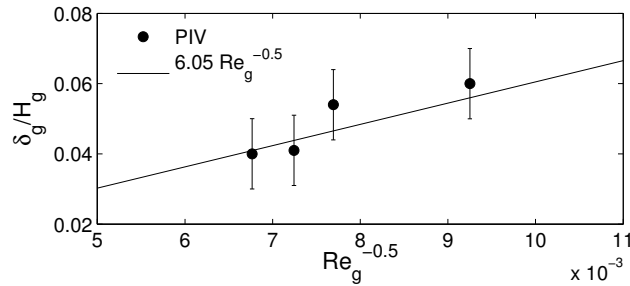


Figure 2 : Single-phase gas flow: evolution of the vorticity thickness just after injection and comparison with the expression of [3].

Finally, the turbulent intensity level in the air-air mixing layer is in the range 10% to 20%, which agrees with the previous results and also with the expectation for a single phase mixing layer (17%).

In the next section, we look at the influence of the drops and/or the interfacial waves on the gas momentum. As a matter of fact, the reduction of the gas velocity downstream injection is mainly due to: (i) the mass conservation in an expanded spray and (ii) an exchange of momentum through a drag term between the continuous phase and the dispersed phase, in the form of drops and interfacial waves. To discriminate between these two phenomena, we need to know the gas velocity in the single-phase flow, case for which, in principle, only the jet expansion can explain the decrease of u_g .

We chose to use the cross-sectional maximum velocity U_{max}^x , taken at the position x as an indicator of the gas velocity decrease. The evolution of U_{max}^x as a function of the downstream distance is presented in figure 3 for two different gas injection conditions.

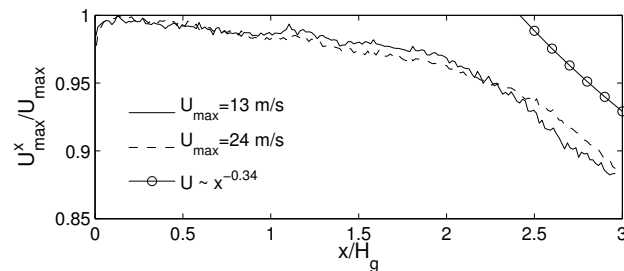


Figure 3 : Single-phase gas flow: cross-sectional maximum velocity at short distance downstream the injection.

For a fully developed plane jet, it can be shown from a momentum integral that U_{max}^x varies as $1/\sqrt{x}$ [9]. In figure 3, the order of magnitude of the power of x is around -0.34 close to $x/H_g=3$. However, in the measurement zone, the mixing layers have not merged yet so the jet is not developed, which explains the discrepancy with the far field theory. Also, the presence of the bottom wall may have some influence on U_{max}^x .

II.2 TWO-PHASE GAS-LIQUID FLOW

As a first step, measurements were carried out at low gas velocity ($U_g=13$ m/s). In those conditions, very few drops are formed whatever the liquid flow rate is, and the air-water interface is weakly deformed. The influence of the water on the evolution of the gas velocity is limited. The spray is displaced upwards, due to the presence of the water layer, but the influence of the water on the evolution of the gas velocity remains weak.

For a higher gas flow rate ($U_g=24$ m/s), the effect is more significant. In figure 4, the gas mean velocity fields, obtained by PIV, are presented.

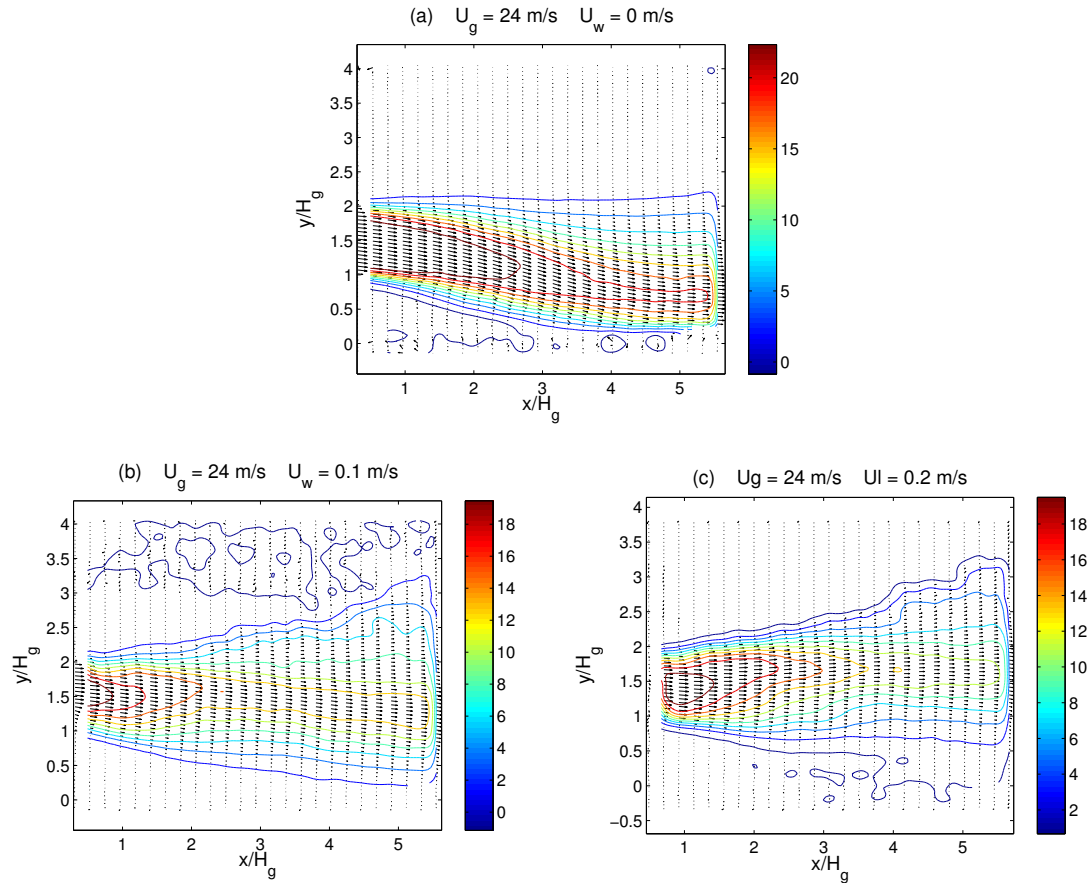


Figure 4 : Gas-liquid flow: mean gas velocity fields and contours of longitudinal velocity at $U_g=24$ m/s.

The single-phase case (figure 4 (a)) is used as a reference. The water velocity is varied between 0.1 m/s (figure 4 (b), $M \approx 70$, where $M = \rho_g U_g / \rho_l U_l$) and 0.2 m/s (figure 4 (c), $M \approx 17$). In this figure, it can be noted that the velocity scale is smaller when water is present, yet the gas valve was kept at the same position as in the single-phase case. This could be due to the momentum exchange between the gas and liquid phase, as explained later. As for the flow structure, the presence of water tends to increase the spray expansion. Particularly, the external mixing layer is shifted upwards, both for the case $U_w=0.1$ m/s and the case $U_w=0.2$ m/s. The potential core of the gas flow seems shorter as more water is injected. This can also be seen on the velocity profiles of figure 5. Close to the injector ($x/H_g=1.2$), the boundary layer in the external mixing layer (air-air) is hardly affected by the presence of the water. At the gas-liquid interface however, the mean velocity gradient is less important as more water is injected, which may be a consequence of the primary instability of the interface [3]. Further downstream, the velocity gradients in the bottom wall region flattens dramatically as the water velocity increases (figure 5 right). The maximum velocity decreases as more water is injected. This could be due to the higher number of drops entrained when more water is injected, however this latter statement should be checked by dedicated experiments.

According to [5], the gas momentum loss due to the entrainment of drops can be roughly estimated as:

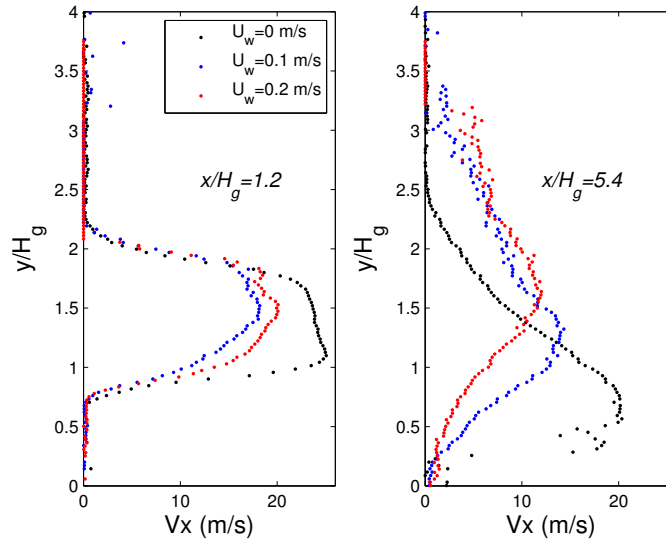


Figure 5 : Gas-liquid flow: profiles of longitudinal gas velocity at $U_g=24\text{m/s}$.

$$\frac{d}{dx} \frac{1}{2} (\rho_g U_g^2) \approx \frac{-n_0 F}{1 - \alpha} \quad (2)$$

where n_0 is the number density of the drops ($\#/m^3$), F is the force exerted by the gas on the drops, and α the liquid volumetric fraction. Considering the flow of small monodispersed drops, F can be assimilated to the Stokes drag for the purpose of a gross estimate:

$$F \approx 3\pi\mu_g d_{mean} V_{mean} \quad (3)$$

where d_{mean} and V_{mean} are the drops mean diameter and velocity respectively. Also, in our conditions of flow, the liquid fraction in the gas-liquid spray remains very low, so that $(1 - \alpha) \approx 1$. Therefore, combining equations 2 and 3, the momentum decay rate can be defined as:

$$\frac{U_g}{U_g(x=0)} \frac{dU_g}{dx} \approx -3\pi n_0 \nu_g d_{mean} \frac{V_{mean}}{U_g(x=0)} \quad (4)$$

For the numerical application, the values needed in equation 4 are taken from [5] at the condition $U_g = 24$ m/s: $n_0 \approx 1.5 \cdot 10^9$, $d_{mean} \approx 160 \mu\text{m}$, $V_{mean}/U_g(x=0) \approx 0.12$. This gives a momentum decay rate of the order of -5 s^{-1} (note that for the condition $U_g=60$ m/s, the momentum decay rate is in the order of -450 s^{-1}). The experimental momentum decay rate can be deduced from the evolution of U_{max}^x for the gas-liquid flow. For short distances downstream ($x/H_g < 3$), the experimental decay rate is in the range -100 to -600 s^{-1} , significantly larger than the value calculated. This may be an indication that in this region, the influence of drops in the gas phase is small, most of the momentum transfer between gas and liquid occurs through interfacial waves.

To conclude, figures 4 and 5 illustrate the interaction between the dispersed phase and the continuous phase. For instance, at $U_g=24$ m/s and $x/H_g > 3$, the maximum velocity of the gas in a gas-liquid flow is 10 to 30% smaller than in a single phase gas flow. In this region, the momentum exchange between the gas and the water is significant. The effect of U_w does not appear obvious. To satisfy the mass conservation of the gas flow, the decrease of the gas velocity downstream due to the dispersed phase must be compensated by a larger expansion of the spray. This is what is observed in figure 4.

As for the velocity fluctuations, it seems that the fluctuations of the longitudinal gas velocity $\langle u' \rangle$ are higher in two-phase flow than in single phase flow: around 35% of the injection velocity, whereas it was at most 20% for single-phase flow. However, this tendency should be confirmed by quantifying accurately the errors made by the PIV algorithm in the calculation of the fluctuations.

III DISPERSED PHASE CHARACTERISTICS

III.1 SPATIAL DISPERSION OF DROPS

Two dimensional fields of the dispersed phase were realized by [5] for the case $U_g=60$ m/s, $M=16$. In figure 6, the local number density flux of drops is plotted as iso-contours, for three size classes of drops: (i) $d < 90\mu\text{m}$, (ii) $90\mu\text{m} < d < 180\mu\text{m}$, (iii) $180\mu\text{m} < d < 270\mu\text{m}$. The spray opening in figure 6 is similar to the opening of iso-temperatures in cryotechnic flames [10]. The half angle of opening is between 15 to 20°, which is larger than the half angle of the spray ($\approx 10^\circ$). Moreover, the drop dispersion depends on their size: the smaller drops are more dispersed than the larger. Intuitively, this can be related to the mechanism of turbulent dispersion applied to a source of particles as a function of their Stokes number St , where $St = \tau_p/\tau_f$, with τ_p and τ_f respectively the relaxation time of the particles and of the surrounding fluid [11]. Following this approach, the particles with low inertia ($St \ll 1$) are more sensitive to the gas turbulence and consequently are more dispersed. However, such an interpretation requires to take account of the drop initial conditions.

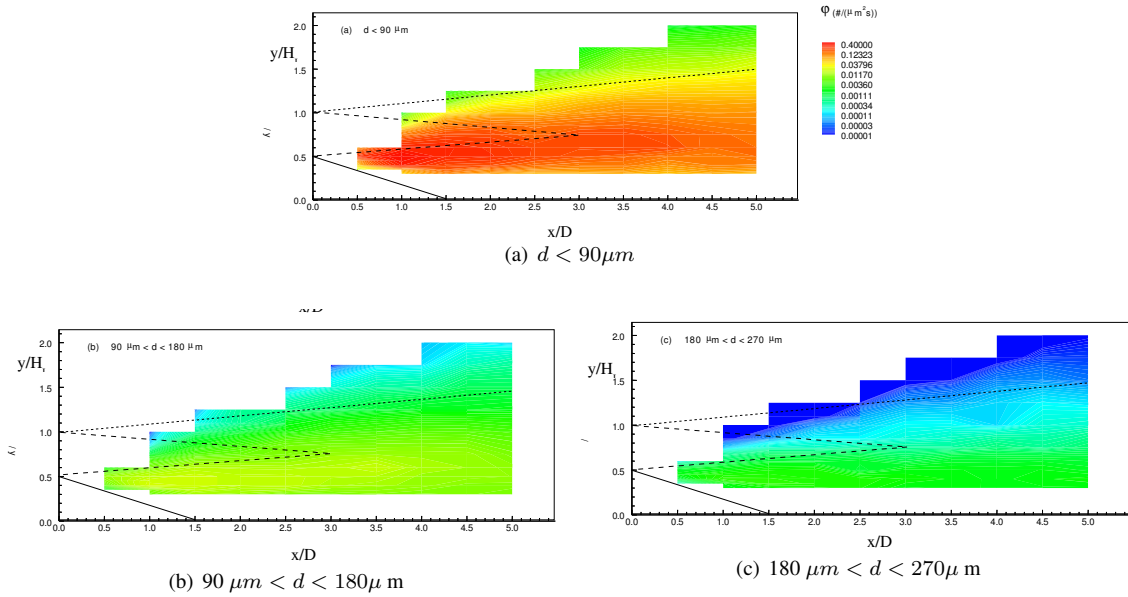


Figure 6 : Gas-liquid flow: contours of the flux of drops φ at $U_g=60$ m/s, $M=16$. After [5].

III.2 DROP MOMENTUM

In this section, we look at the equation of motion of drops subjected to the drag. A simple drag model is applied, neglecting the effect of the drops on the gas flow (“one-way coupling”). Considering gravity and drag, the momentum conservation equation reads:

$$m_d \frac{d\vec{v}_{drop}}{dt} = m_d \vec{g} - \frac{1}{2} C_D \pi \frac{d^2}{4} \|\vec{U}_g - \vec{v}_{drop}\| (\vec{U}_g - \vec{v}_{drop}) \quad (5)$$

where \vec{v}_{drop} is the drop velocity. By restricting the study to the case of drops travelling horizontally, equation 5 can be projected:

$$\frac{dv_{drop}}{dt} = \frac{3}{4} C_D \frac{\rho_f}{\rho_d} \frac{\Delta U^2}{d} \quad (6)$$

where ΔU is the velocity difference between the drop and the surrounding gas. For $Re < 800$, with $Re = (U_g - v_{drop})d/\nu_g$, the expression from Schiller & Nauman is used for the drag coefficient:

$$C_D = \frac{24}{Re} (1 + 0.15 Re^{0.687}) \quad (7)$$

In this case, equation 6 becomes:

$$\frac{dv_{drop}}{dt} = \frac{f}{\tau_p} \Delta U \quad (8)$$

where $f = 1 + 0.15Re^{0.687}$ is the friction coefficient. For $Re > 800$, the expression of Gilbert can be used:

$$C_D = 0.48 + 28Re^{-0.8} \quad (9)$$

By using the images from the high-speed camera, it is possible to individually follow the drops and thus to calculate their acceleration by way of lagrangian derivative dv_{drop}/dt . This value is then compared to that of equation 6, where C_D is calculated according to equation 7 or 9. In figure 7, 11 trajectories of drops travelling in the horizontal direction and without initial velocity have been analysed. The sample of drops were tracked in a zone downstream injection for which $1 < x/H_g < 5$, and the range of size is between 0.07 mm and 2 mm. For the same conditions, the mean drop size d_{mean} is approximately 0.5 mm according to [5]. The gas velocity at the injection is $U_g = 24$ m/s and we chose $\Delta U = 20$ m/s ± 5 m/s (dashed lines).

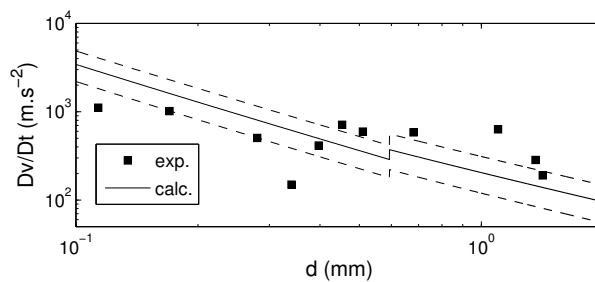


Figure 7 : Acceleration of drops travelling horizontally, without initial velocity, in the zone $x/H_g \in [1;5]$. Comparison between measurements by high-speed camera and equation 6. The discontinuity around $d = 0.6$ mm is due to the transition between equations 7 and 9.

It can be seen that the order of magnitude of the measurements is in good agreement with this simple model, and, in spite of the uncertainties, the tendencies are respected. Therefore, this approach is suited for the case of drops trapped in the core of the gas jet without initial velocity, however the proportion of these drops among the full population of drops needs to be determined.

III.3 TRAJECTORIES AND ANGLES OF EJECTION

In figure 8, some drop trajectories originating from different ligament bursts obtained with the high-speed camera are displayed. The gas field at the same conditions is superimposed.

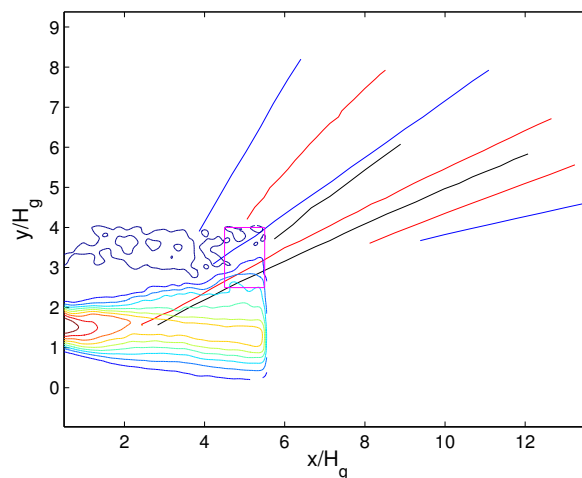


Figure 8 : Gas-liquid flow: example of drop trajectories at $U_g \approx 24$ m/s, $U_w \approx 0.1$ m/s and comparison with the corresponding PIV field.

This figure emphasizes the importance of the drop inertia: their trajectories appear fairly straight, the gas jet does not significantly deviate them. On the other hand, it can be noticed that there is a large range of ejection angle. Additional measurements using PTV have shown that at the end of the liquid intact length, most of the ejection angles are in the range 0 to 40°, however it occurs occasionally that the drops are ejected with angles as high as 60° (figure 9). This has also been observed by [8].

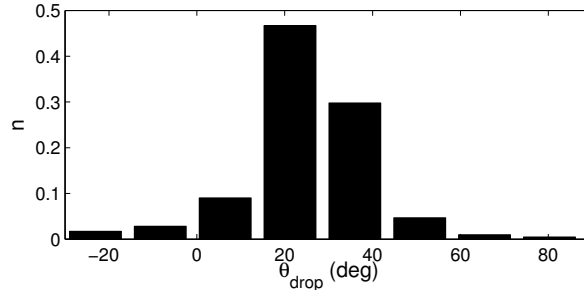


Figure 9 : Gas-liquid flow: normalized distribution of the displacement angle of drops measured by PTV, in a rectangular zone depicted in figure 8. The mean angle in this zone is 22°.

The application of the simple model presented in section III.2 does not seem well adapted to describe the behaviour of drops with large angle of ejection. By looking at figure 8, it can be supposed that these drops, with a large incidence, travel through the gas core and end up in the external mixing layer, where they are not accelerated by the gas. Therefore, the initial conditions of the drops should be considered to explain the spatial distribution of that population.

IV SPRAY DISPERSION

The results of section IV are now re-examined in the light of the previous considerations. We are interested in identifying which mechanism dominates in the dispersion of drops, as seen in figure 6 in terms of drop flux. Two approaches can be opposed: the approach only taking account of turbulent dispersion, and the deterministic approach, which considers the role of the initial conditions of the drop on its future trajectory. In this section, both cases will be discussed and applied to the evolution of the drop concentration.

IV.1 TURBULENT DISPERSION APPROACH

In the following, a simple analysis will be carried out based on the turbulent diffusion model developed by [11] for gas-liquid annular flow. To apply such a model, it is necessary to assume that the drop is smaller than the length scale of turbulence, so that the drop is entrained by the smallest eddies.

The general convection-diffusion equation describing the deposition of particle (drops) in a turbulent flow can be written as:

$$\frac{\partial \alpha}{\partial t} + \vec{\nabla} \cdot (\vec{u} \alpha) = \vec{\nabla} \cdot (D_p \vec{\nabla} \alpha) \quad (10)$$

Where \vec{u} , α and D_p represent respectively the (total) convective velocity, the drop concentration, and the drop diffusion coefficient. The following assumptions are made:

- steady state,
- particle-particle interactions are ignored, so there are no birth or death of drops by collisions,
- D_p is uniform in a vertical section.

To further simplify, we will assume that α is only a function of the vertical axis. Indeed, based on the data of [5], it has been shown that there is a weak longitudinal variation of the spray. Equation 10 can then be written as:

$$v \frac{d\alpha}{dy} = D_p \frac{d^2 \alpha}{dy^2} \quad (11)$$

where v is the convective velocity of the drops in the vertical direction. Equation 11 shows the balance between the convective velocity of drops and the turbulent diffusion. In developed annular flow, v was taken as the terminal velocity of drops due to gravity g ([11, 12]):

$$v_{grav} = g\tau_p \quad (12)$$

where τ_p is the drop relaxation time, based on Stokes drag:

$$\tau_p = \frac{\rho_p d^2}{18\mu_f} \quad (13)$$

with ρ_p the density of the particles (water) and μ_f the dynamic viscosity of the surrounding fluid (gas). For the case of gas liquid atomization, the assumption of developed flow is not valid, and the initial velocity of the drops during the primary atomization has to be taken into account. Particularly, the entrainment velocity u_e , which is the vertical component of the velocity at the ligament breakup, is of importance. According to [8], the drops are ejected at approximately 45° from the horizontal axis, so that the entrainment velocity is close to the breakup convective velocity U_c , with U_c along x given by [13]:

$$U_c = \frac{\sqrt{\rho_g}U_g + \sqrt{\rho_l}U_l}{\sqrt{\rho_g} + \sqrt{\rho_l}} \quad (14)$$

where subscripts g and l stand for gas and liquid respectively. Note that the mean angle of ejection found in section III is smaller than 45° , however it does not change the order of magnitude. Hence the total convective velocity of drops in equation 11 is written:

$$v = U_c - v_{grav} \quad (15)$$

By integration of equation 11:

$$\alpha = \alpha_0 \exp\left(-\frac{v}{D_p}y\right) \quad (16)$$

The particle diffusivity D_p is modelled by [12] using the surrounding fluid (gas) diffusivity D_g :

$$D_p = \gamma_v \gamma_{grav} D_g \quad (17)$$

where the coefficients γ_v and γ_g stand for the effect of crossing trajectories due to inertia and gravity respectively. According to [12], the term γ_{grav} can be neglected ($\gamma_{grav}=1$) as long as the convective velocity of drops v is significantly smaller than the fluid fluctuating velocity v'_g , which we will assume. The term γ_v is written ([11]):

$$\gamma_v = \frac{1}{\sqrt{1+S}} \quad (18)$$

where $S = \tau_p/T_L$ is the Stokes number based on τ_p and the integral time scale of the fluid T_L . This scale was calculated based on the macroscopic length and velocity scales. The fluid diffusivity is expressed by [14] as:

$$D_g = \langle (v'_g)^2 \rangle T_L \quad (19)$$

The previous analysis is now applied to calculate the concentration profiles and compare with the experimental data from [5]. The same mean size classes as in figure 6 are used. For the estimation of the r.m.s. velocity of the gas phase, it was seen from the PIV measurements (section II) that the turbulence intensity level is higher in the presence of the drops. Therefore, the usual expression $\sqrt{\langle (v'_g)^2 \rangle} = 0.17U_g$ obtained for a single phase mixing layer ([15]) is replaced by $\sqrt{\langle (v'_g)^2 \rangle} = 0.35U_g$ for the present conditions. The characteristic scales are summarised in table IV.1.

From the experimental results, the quantity v/D_p is easily found, it corresponds to the slope of the concentration profiles when modelled according to equation 16. The comparison between the measured v/D_p and the calculated v/D_p using equations 15 to 19 is given in figure 10. A sample of downstream distances is used. It appears that the best agreement is found for concentration profiles taken at around $x/H_g = 4$, which is beyond the liquid intact length.

Using equations 14 and 15 to get the total convective velocity as a function of the drop size, the particle diffusivity can be calculated from the measurements, from which the concentration is deduced.

Height of injector	L	0.01	m
Gas velocity	U_g	60	m.s^{-1}
Liquid velocity	U_l	0.51	m.s^{-1}
gas r.m.s. velocity	$\sqrt{\langle (v'_g)^2 \rangle}$	21	m/s
Integral time scale	T_L	$1.7 \cdot 10^{-4}$	s
Fluid diffusivity	D_g	$7.35 \cdot 10^{-2}$	$\text{m}^2.\text{s}^{-1}$
Breakup convective velocity	U_c	2.81	m.s^{-1}

Table 1 : Characteristics scales for gas-liquid flow

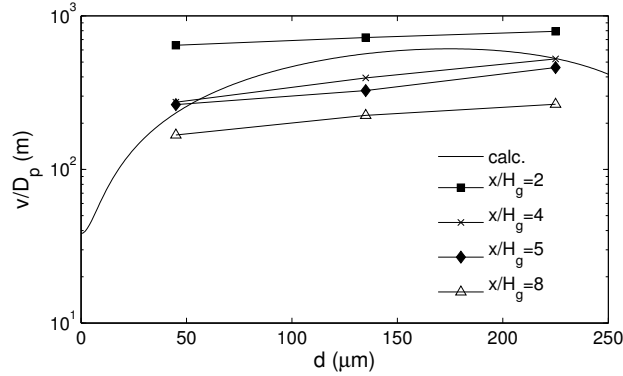


Figure 10 : v/D_p measured from concentration profiles and calculated using equations 15 to 19

The experimental normalised concentrations are compared to the calculated concentrations in figure 11 at one downstream distance. The initial concentration α_0 has been set as the value of α at $y/H_g=0.6$, which was the minimum height for the optical probe measurements.

As can be seen, the order of magnitude is reasonable. However the general trend is not respected, *i.e.* the slopes of the concentration profiles do not vary monotonously with the class size. This comes from the choice of the total convective velocity which is not adequate.

The inverse length scale v/D_p should be a monotoneous function of the drop size, where as the calculated inverse length scale using equations 13, 14 and 15 displays a maximum in the interval of study (figure 10). A possible improvement is to set the breakup convective velocity in equation 14 as a variable of the drop size. Still, the limited number of class size makes the comparison with the calculations hazardous.

IV.2 DETERMINISTIC APPROACH

To help characterizing the drop dispersion, it is worth to measure the dispersion of a passive tracer, that is to say with low inertia and no initial velocity, at the same flow conditions if possible. The PIV tracers (water + glycerin) can be used for this purpose. The dispersion of PIV tracers have been measured with an image processing algorithm. Due to the choice of this algorithm and the experimental constraints, it was only possible to study the case of a single-phase flow of gas, at a lower velocity than that of figure 6: $13 \text{ m/s} < U_g < 30 \text{ m/s}$. However some qualitative informations can be noticed.

In figure 12, iso-contours of the PIV tracers concentration are represented. The gas injection is located in the region $x/H_g=0, y/H_g \in [1;2]$. As can be seen, the particles remain confined close to the bottom wall ($y/H_g=0$). In the rest of the space, the particle concentration is very dilute. The decrease of concentration in the longitudinal direction is probably due to the evaporation of some part of the tracers, and the weakening of the laser sheet intensity in this region. According to figure 12, at relatively short distances downstream ($x/H_g < 8$), the turbulent diffusion process is rather limited and the particle are not much dispersed. Most of them are transported in the core of the gas jet. Further downstream, it has been observed that the particle migrate in the external mixing layer and finally dispersed to the whole space by diffusion and recirculation. Similar results were obtained for gas velocities up to $U_g = 30 \text{ m/s}$.

By comparing figures 6 and 12, it appears that the drop dispersion is fairly different from that of the PIV tracers. Therefore, the initial conditions of motion of drops seems to be a determinant aspect for some

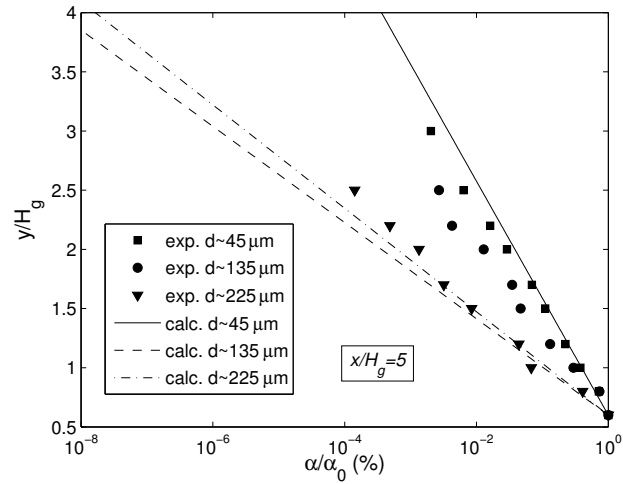


Figure 11 : Concentration profile at $x/H_g=5$

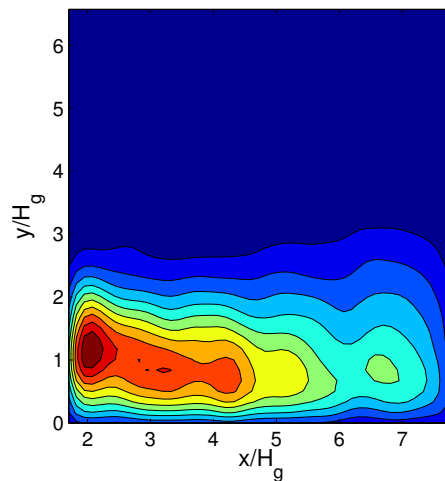


Figure 12 : Single phase gas flow: mean concentration of particles in arbitrary units, at $U_g = 13$ m/s.

population of drops. Once the drop is ejected, its inertia dictates its displacement. As a consequence, a systematic analysis of the drop ejection statistics should be undertaken.

V CONCLUSION

An experimental study of the spatial evolution of a gas-liquid mixing layer has been carried out. Measurements of the gas velocity were performed by PIV. For a low gas flow rate, the decrease of the gas velocity downstream can be explained by the spray expansion. Some momentum exchange occurs in the external mixing layer. At higher gas flow rate, the air-water interface deforms and some drops are stripped off and entrained in the gas phase. These obstacles in the gas flow provoke a faster decrease of the gas velocity downstream, by momentum transfer between the dispersed and the continuous phase.

As for the drops, the data of [5] provide some information about their dispersion, which depends on their size. The dispersion can be the result of the transport by the turbulent gas field of the drops produced in the primary atomisation zone. However, some measurements using high-speed camera underline the importance of the initial conditions of the drop at the moment of its formation. Two extreme cases can be distinguished: (i) drops that have no initial velocity are accelerated by the drag and remain in the core of the gas jet (ii) drops with a high vertical component of their initial velocity are weakly influenced by the gas field. Additional measurements are needed to evaluate the proportion of drops in those categories, and, in

general, to have correlated statistics on the drop diameter, initial angle and initial velocity.

As a matter of fact, the initial conditions of drops seem to play an important role in the dispersion. Therefore, modelling efforts should be aimed at qualifying and reproducing the ligament break up events in the primary atomisation zone.

REFERENCES

- [1] A Vallet, AA Burluka, and R Borghi. Development of a eulerian model for the atomization of a liquid jet. *Atomization and sprays*, 11:619 – 642, 2001.
- [2] S Zurbach, JL Thomas, and M Sion. Défis technologiques et industriels pour la combustion dans les moteurs fusée. In *GdR Combustion dans les moteurs fusées*, 2001.
- [3] F Ben Rayana. *Contribution à l'étude des instabilités interfaciales liquide-gaz en atomisation assistée et tailles de gouttes*. PhD thesis, Institut National Polytechnique de Grenoble, 2007.
- [4] M Hong, A Cartellier, E Hopfinger, and JP Matas. Some aspects of spray formation and development in the near field of two-phase coaxial injectors. In *Proceedings of the 11th Workshop on Two-Phase Flow Predictions*, Merseburg, Germany, 2005.
- [5] M Hong. *Atomisation et mélange dans les jets coaxiaux liquide-gaz*. PhD thesis, Institut National Polytechnique de Grenoble, 2003.
- [6] E Barrau, N Rivière, C Poupot, and A Cartellier. Single and double optical probes in air-water two-phase flows: real time signal processing and sensors performances. *Int. J. Multiphase Flow*, 25:229 – 256, 1999.
- [7] M Hong, A Cartellier, and E Hopfinger. Characterization of phase detection optical probes for the measurement of the dispersed phase parameters in sprays. *Int. J. Multiphase Flow*, 30:615 – 648, 2004.
- [8] L Raynal. *Instabilité et entrainement à l'interface d'une couche de mélange liquide-gaz*. PhD thesis, Université Joseph Fourier, Grenoble, 1997.
- [9] AA Townsend. *The structure of turbulent shear flow*. Cambridge University Press, 1956.
- [10] M Juniper. *Structure et stabilisation des flammes cryotechniques*. PhD thesis, Ecole Centrale Paris, 2001.
- [11] B Mols and RVA Oliemans. A turbulent diffusion model for particle dispersion and deposition in horizontal tube flow. *Int. J. Multiphase Flow*, 24(1):55 – 75, 1998.
- [12] B Mols, I Mittendorff, and RVA Oliemans. Results from a two-dimensional turbulent diffusion-model for dispersion and deposition of droplets in horizontal annular dispersed gas/liquid flow. *Int. J. Multiphase Flow*, 26(6):949 – 975, 2000.
- [13] PE Dimotakis. Two-dimensional shear layer entrainment. *AIAA*, 24(11):1791 – 1796, 1986.
- [14] GI Taylor. Diffusion by continuous movements. In *Proceedings of the London Mathematical Society*, London, UK, 1921.
- [15] AKMF Hussain and MF Zedan. Effects of the initial condition on the axisymmetric free sheer layer: effects on the initial momentum thickness. *Phy. Fluids*, 21(7):1100 – 1112, 1978.